# On the influence of crystallographic texture on HIC in low carbon steels

**V. Venegas[1], F. Caleyo[1], J. M. Hallen[1] and T. Baudin[2]**

[1] DIM-ESIQIE, Instituto Politécnico Nacional, México D.F. 07738, México.
[2] LPCES, Université de Paris Sud, Orsay 91405, France.

Contact e-mail address: fcaleyo@email.com.

**Abstract**

This work presents the results of investigations aimed at determining the influence of crystallographic texture on hydrogen induced cracking (HIC) in low carbon steels. X-ray diffraction texture measurements have been conducted on specimens affected by HIC samples and Orientation Imaging Microscopy (OIM$^{TM}$) has been used to conduct microtexture and mesotexture analyses on these samples. Based on the results presented in this work, it can be concluded that the susceptibility of low carbon steels to HIC can be reduced through crystallographic texture control and grain boundary engineering.

## 1. Introduction

Hydrogen induced cracking (HIC) occurs in low strength steels exposed to aqueous $H_2S$ environments. The two major strategies to improve HIC resistance are the reduction in the steel sulfur content and the control of inclusion morphology [1]. These strategies, however, have proven not to be completely effective to prevent HIC in severe conditions [1, 2].

Crystallographic texture can be effectively controlled during the steel making process [3] and is expected to play a key role in HIC because it can determine the availability of low resistance paths for crack propagation. Verdeja *et al*. [2] have shown that large hot rolling pass strain schedules produce {100}-{113}-{112}//ND textures which increase HIC susceptibility in structural steels. Recently, Venegas *et al.* [4] used OIM to study the role of crystallographic texture on HIC.

The mechanisms observed for HIC are those of hydrogen-enhanced decohesion, hydrogen-enhanced plasticity and absorption-induced dislocation emission [5]. They all depend strongly on the crystallographic orientation of the material at crack tips. Therefore, if texture is considered with regard to HIC, it is best to have access to the microtexture and mesotexture of the material rather than considering only its macrotexture.

This work presents the results of ongoing investigations aimed at determining the influence of microtexture, mesotexture and macrotexture on HIC in low carbon steels for

sour-service piping. HIC samples of two steels were investigated using X-ray texture measurements and OIM. The first steel a low strength API 5L X46 and the second is a low sulfur ASME A106. The microtexture measurements have allowed to study how each one of the texture components found in these steels contribute to HIC propagation. The mesotexture analysis has allowed evidencing the influence of grain boundary statistic on the availability of weak paths for intergranular HIC propagation.

## 2. Experimental

HIC samples were obtained from two steels for which the composition is shown in Table 1. Samples of steel A were taken from an HIC damaged section retired from a 610 mm (24-inch) diameter API-5L-X46 pipeline of 12 mm thickness which transported wet sour gas. Plates of steel B were taken from a new 610 mm, 12 mm thickness, ASME A106 line pipe. From these plates, HIC samples were produced by following the NACE TM0284 standard.

The texture of both steels was measured using X-ray diffraction at central layer on the rolling plane (containing the rolling RD and transverse TD directions). Three incomplete pole figures: {110}, {200} and {111}, were measured to determine the orientation distribution functions (ODFs) of the samples. Electron backscattering diffraction (EBSD) was used to perform microtexture measurements on HIC cross sections containing the TD and normal ND direction. Individual grain orientations were determined on a hexagonal grid with step size ranging from 0.1 to 3 μm. For each measured HIC region, the distribution of individual grain orientations and of EBSD pattern quality (IQ) and grain misorientation spread values were mapped. Grain boundaries were defined by the presence of point-to-point disorientations greater than 2° and were classified into: (i) coincidence-site-lattice (CSL), (ii) low-angle (LABs) and (iii) high-angle (HAB) boundaries.

Table 1. Chemical composition of the investigated steels (in wt%).

| Steel | C | Mn | S | P | Si | Cu | Cr |
|---|---|---|---|---|---|---|---|
| A | 0.212 | 1.334 | 0.032 | 0.028 | 0.037 | - | 0.009 |
| B | 0.085 | 0.916 | 0.009 | 0.017 | 0.252 | 0.272 | 0.011 |

## 3. Results

### *3.1 Metallography*

Figure 1a shows a SEM micrograph taken from the TD-ND section of an HIC sample of steel B. This material shows a banded pearlite/ferrite microstructure with a pearlite proportion of about 8% and a grain size close to 15 μm. Steel A also shows a pearlite/ferrite microstructure, yet the grain size and pearlite proportion were found to be 20 μm and 30%, respectively. Steels A has elongate (type II) MnS inclusions which were found to be the main sites for HIC nucleation. In steel B, the MnS inclusions are much less numerous and

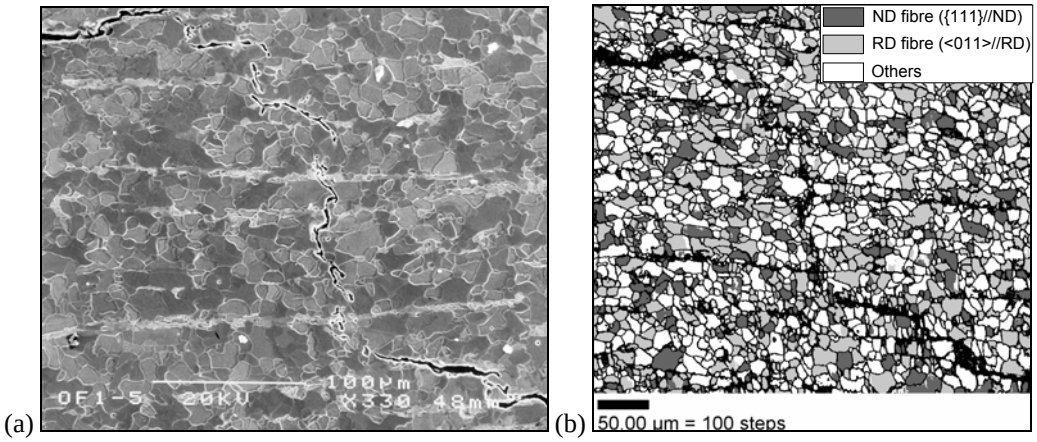


Figure 1. (a) SEM micrograph and (b) EBSD-derived orientation map taken from the TD-ND section of an HIC sample of steel B. Grains within 15° of each texture fibre are shaded as marked in legend given in (b).

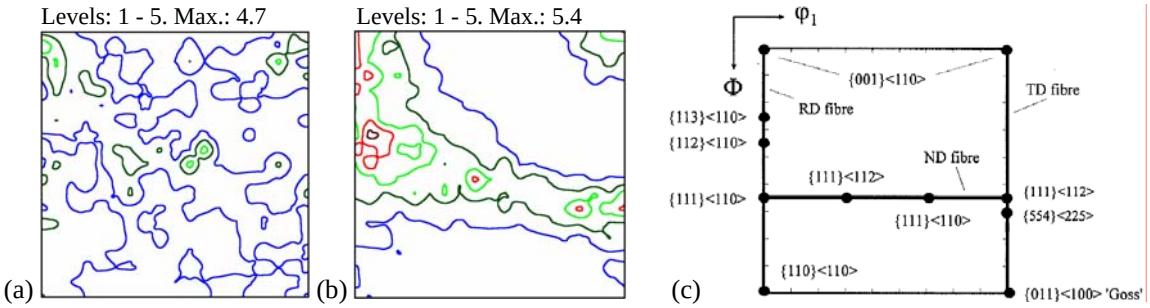


Figure 2. $\varphi_2$=45° sections of the ODFs of steels A (a) and B (b). (c) Key to the main steel texture components.

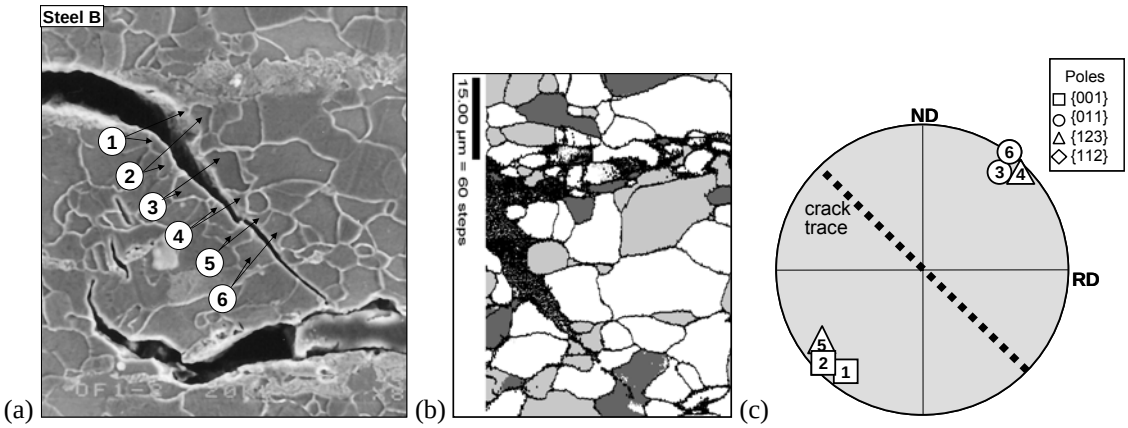


Figure 3.Intragranular HIC propagation in steel B. (a) SEM micrograph. (b) EBSD-derived orientation map. (c) Position of the poles of the most probably active cleavage and slip planes, relative to the crack trace.

have spherical shape so that HIC nucleated mainly at ferrite/pearlite interfaces in this steel.

In both materials, HIC cracks grow parallel to the rolling plane following intergranular and transgranular paths. In many cases, the tips of approaching cracks deflect toward each other in the ND, leading to crack coalescence and stepwise propagation. The microscopic details of this latter process are investigated in Section 3.3.

### *3.2. Macrotexture*

Figure 2 shows the $\varphi_2 = 45°$ section of the ODFs (in Euler space) of both materials. Steel A has a nearly random texture typical of low carbon steels finished using an austenitic hot rolling strategy [2]. However, a weak departure from randomness is observed at orientations within 15° of the ideal rotated cube {001}<110> and {112}<110> orientations. The most important feature in this texture is the weakness of the {111}//ND fibre. In contrast, steel B displays a strong texture characteristic of recrystallized (warm) ferrite-rolled bcc materials. This consists of a dominant <110>//RD fibre together with a complete {111}//ND fibre. The ODF maximum is observed at the {112}<110> component.

### *3.3 Microtexture*

Figure 1b shows the EBSD-derived orientation map of the HIC region shown in Fig. 1a. The microstructural data extracted from the orientation maps agreed with that obtained using conventional metallography and X-ray diffraction. The microtexture analyses did not evidence the presence of local texture heterogeneities such as orientation clustering.

*Role of microtexture on crack path*: This investigation corroborates previously published results [2, 4, 5] showing that transgranular HIC crack propagation takes place in most cases through cleavage and slip-band fracture (Fig. 3). In both steels, cracks were found to propagate transgranularly along the {001} planes which contributed to the development of HIC parallel to the rolling plane and to crack deflection in the ND direction (Fig. 3c). Transgranular propagation in the {011}, {112} and {123} slip planes was observed mainly at deflected crack ends (Fig. 3c). The low resistance cleavage paths for transgranular HIC in the rolling plane were found to be provided by grains with orientations within 15° of the ideal {001}//ND fibre. Crack deflection in the ND was found to be associated with transgranular propagation along cleavage and slip planes in grains with orientations of the {111}//ND, <011>//RD and {001}//ND fibres.

The relationship between grain orientation and crack path is further assessed in Fig. 4. The $\varphi_2 = 45°$ section of the ODF computed from the orientations of more than 1800 grains along crack paths in steel A is shown in Fig. 4a. HIC propagation is mainly associated with {001}//ND oriented grains. This can be related to the fact that cleavage propagation in the rolling plane is enhanced in a material with a large number of these grains. It can also be postulated that (tilt) low-angle boundaries between neighboring {001}/ND grains provide weak intergranular paths along which cleavage propagation can occur.

Figure 4b shows the $\varphi_2 = 45°$ section of the ODF computed from the individual grain orientations of more than 600 grains located immediately ahead (see Fig. 4c) of several crack tips in steel A. This figure shows that the probability that HIC arrest or/and deflect in the ND increases when crack fronts encounter grains with orientations within the {111}//ND, {112}//ND and {011}//ND fibres.

Therefore, it can be concluded that the presence of rotated cube {001}//ND grains favors HIC in the rolling plane while the occurrence of the {111}//ND, {112}//ND and {011}//ND orientations impedes it by increasing the proportion of high resistance paths for crack propagation. This latter can be attributed to the lack of suitably oriented cleavage planes in the grains having these latter orientations. Moreover, the driving force required to crack extension through fracture along slip planes, *e.g*. in {011}//ND oriented grains, is relatively high as to reduce the role of this latter mechanism to HIC.

*HIC-induced plastic strain:* The distribution of plastic strain around the HIC cracks was investigated by mapping the EBSD pattern quality parameter, which decreases with increasing plastic strain. Figure 5 shows the SEM micrograph and the EBSD pattern quality map of a region containing two approaching cracks in steel A. The cracks overlap and deflect in the ND direction but do not coalesce. Such deflection occurs through transgranular cleavage along {001} planes (grains 1a and 1b) and the region between the crack tips shows a large plastic strain.

The influence of microtexture on the plastic strain related to HIC is best assessed by observing the resulting in-grain orientation heterogeneities. Figure 5c reveals that the grains between the overlapping cracks show the largest in-grain orientation scatter, which reaches 11° for grain 1. In the interaction zone, the deformation occurs heterogeneously by the slip activity induced by the mixed mode stress [6] that develops between the cracks as they approach each other (stage I) and overlap (stage II). This stressing condition leads to the deflection of close spaced cracks and triggers crack nucleation between crack tips [6].

Figure 6 helps to explain how plastic deformation occurs in grain 1, whose orientation is close to {111}<121>. Figure 6a shows that a large cumulative misorientation develops along this grain as a result of its deformation by slip under the influence of grain-to-grain interaction. Yet, the nearest neighbor misorientation profile crosses low-angle boundaries not greater than 5°. This behavior was observed for all the grains marked in Fig. 6c.

The inset in Fig.6a shows the inverse pole figure of the shear axis (SA) in grain 1. In this figure, SA-I and SA-II refer to the shear axes identified for stages I and II of the interaction process, respectively. The large cumulative misorientation observed in grain 1 is related to the rotation of the crystal <111> slip direction towards SA-I at point C, and towards SA-II at point A. These lattice rotations align the traces of the active {110}, {112} and {123} slip planes with the shear planes (SP) that can be defined for both interaction stages (see Fig. 6b). This indicates that the deformation of grain 1 started when the cracks were close enough as to induce a shear stress greater than the critical shear stress and that this deformation continued during crack overlapping. The lattice reorientation observed in

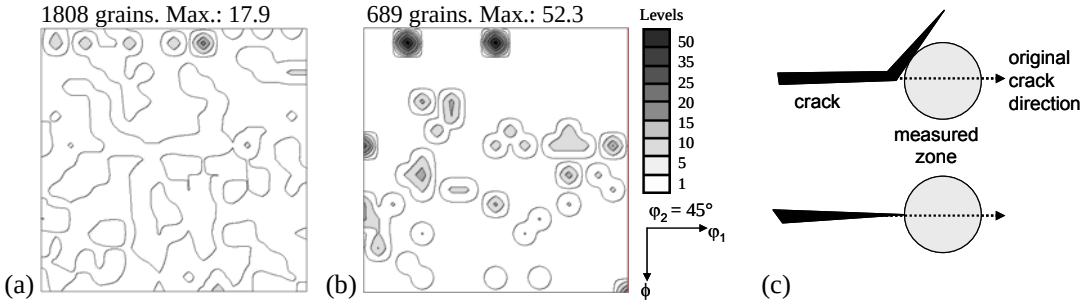


Figure 4. $\varphi_2 = 45°$ sections of the ODFs computed from individual grain orientations in steel A. (a) Along crack paths. (b) Immediately ahead of crack tips (along the original crack direction) as shown in (c).

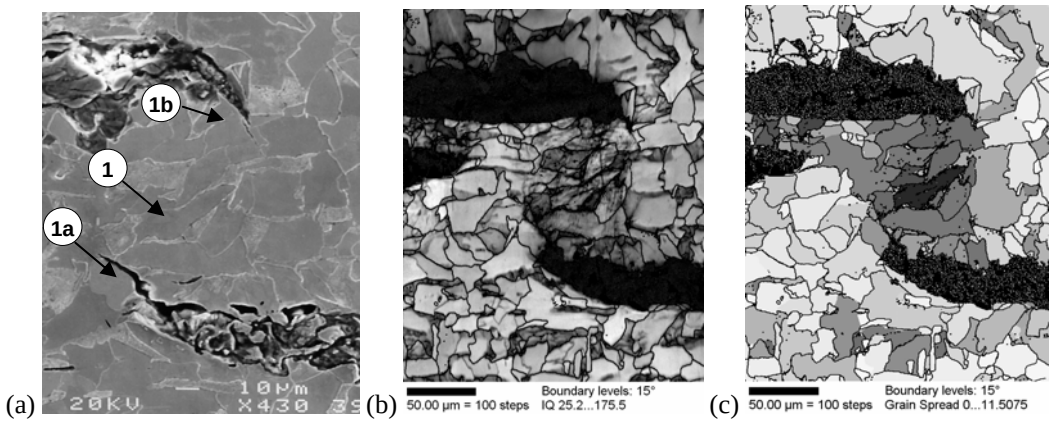


Figure 5. Two interacting cracks in steel A. (a) SEM micrograph. (b) EBSD pattern quality map. (c) Grain average misorientation spread distribution. In (b) and (c), strain increases with the darkness of the gray scale.

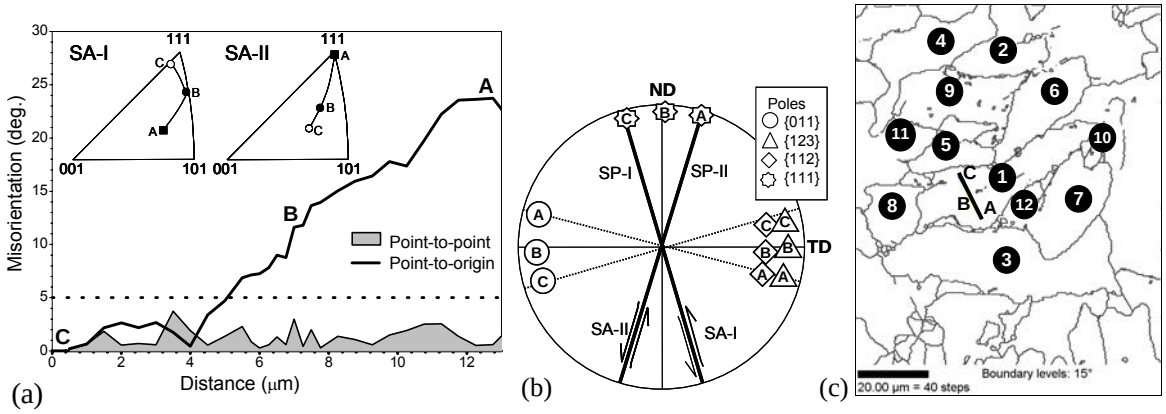


Figure 6. Lattice reorientation by plastic deformation. (a) Misorientation profile along line A-C. (b) Poles of the active slip systems at points A, B and C (relative to the shear stress axes). (c) Key for grain identification.

grains 6–9 and 12 indicates that these grains deformed plastically most probably during stage I, while grains 2–5, 10 and 11, deformed during stage II.

The enhanced slip activity observed in the region between the interacting cracks decreases the driving force for crack propagation and also the probability of crack coalescence due to the shear stress relaxation by plastic deformation [6]. It is important to stress that this will occur more frequently in grains with orientations of the {111}//ND fibre because they have more favorably oriented slip systems for large plastic deformation by extensive slip during both crack interaction stages.

### *3.4 Mesotexture*

The influence mesotexture on HIC was investigated by determining the statistical distribution of grain boundaries along crack paths and in non-cracked regions. Figure 7 shows the proportion of low-angle (LABs), high-angle (HABs) and coincidence-site-lattice (CSL) boundaries along HIC paths and in regions where HIC did not develop.

The HIC paths have associated higher proportions of low-angle and of high-angle boundaries than the regions where HIC did not develop. They also show the lowest proportion of coincidence boundaries. This indicates that intergranular HIC occurs mainly along high energy boundaries while coincidence and low-angle boundaries provide a reduced number of crack paths. Note that the $\Sigma 3^n$ boundaries in this material should be classified as high-angle boundaries since they are most probably not generated by twinning. An example of a "texture induced" non-coherent twin boundary is one shared by a grain with $(111)[1\bar{1}0]$ orientation and its $(111)[0\bar{1}1]$ neighbor. The relatively high proportion of low-angle boundaries observed along crack paths was related to intergranular crack grow along boundaries between neighboring {001}//ND grains. This result confirms that the presence of a strong {001}//ND fibre texture increases the steel susceptibility to HIC.

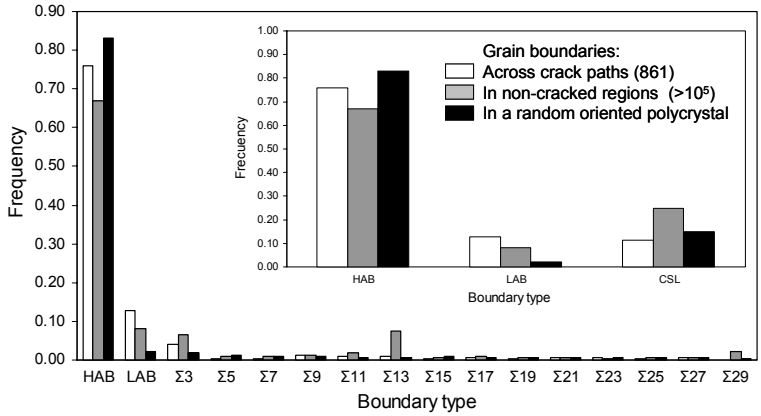


Figure 7. Grain boundary statistic along crack paths and in non-cracked regions in steel A.

The mesotexture in the non-cracked regions shows the highest proportion of coincidence boundaries. This is especially noticeable for the Σ13s (mainly Σ13b), Σ11s and Σ29s (mainly Σ29a). The high proportion of Σ13b boundaries observed in these regions was related to the presence of a relatively large proportion of grains with {111}//ND orientations. Note that the relationship between the {111}<110> and {111}<121> orientations is within 3° of the ideal misorientation that defines a Σ13b boundary.

Furthermore, it has been reported [7] that the energy of low-angle boundaries with misorientation axes close to <001> is higher than the energy of those with rotation axes close to <111>. Thus, a steel with a strong {111}//ND fibre texture should show an increased resistant to HIC because of the increased presence of coincidence-site-lattice boundaries and of low-angle boundaries with the lowest possible energy.

## 4. Conclusions

This work confirms the feasibility of improving the HIC resistance of steels for sour-service piping through crystallographic texture control and grain boundary engineering. Controlled rolling schedules can be proposed in order to induce in these steels a texture dominated by the {112}//ND, {111}//ND and {011}//ND fibres. Such a texture is expected to reduce the probability of HIC by: (i) reducing the number of available transgranular and intergranular low resistance cleavage paths provided by the {001}//ND oriented grains, (ii) decreasing the probability of crack coalescence and stepwise HIC propagation and (iii) increasing the number of high resistance intergranular crack paths provided by coincidence-site-lattice boundaries and by low-angle boundaries with the lowest possible energy.

## Acknowledgements

The author whish to thank D. Solas and E. S. Valladares for measuring the X-ray pole figure of the investigated steels and for processing the OIM data, respectively.

## References

1. Elboujdaini M. (2000) In *Uhlig's Corrosion Handbook* (Ed. Winston Revie. R.), John Wiley & Sons Inc. pp. 205-220.
2. Verdeja, J.I., Asensio, J. and Pero-Sanz, J.A. (2003) *Mater. Character.* **50**, 81-86.
3. Ray, R.K., Jonas, J.J., Butrón-Guillén, M.P. and Savoie, J. (1994) *ISIJ* **34**, 927-942.
4. Venegas, V., Caleyo, F., González, J., Baudin, T., Hallen, J. and Penelle, R. (2005) *Scripta Mat*. **52** 147-152.
5. Lynch, S.P. (2003) In *Hydrogen Effects on Materials Behavior and Corrosion Deformation* (Ed. Moody *et al.*), The Mineral, Metals & Materials So. pp. 440-466.
6. Wang, Y-Z., Atkinson, J.D., Akid, R and Parkins, R.N. (1996) *Fatigue. Fract. Eng. Mater. Struct*. **19**, 427-439.
7. Yang, C.C. Rollet, A.D. and Mullins, W.W. (2001) *Scripta Mat*. **44** 2735-2741.